Journal of Nuclear Materials 495 (2017) 306–313

Contents lists available at ScienceDirect

Journal of Nuclear Materials

journal homepage: www.elsevier.com/locate/jnucmat

# Creep behaviors and microstructure analysis of CNS-2 steel at elevated temperatures and stresses

Yingxue Chen [a], Yong Zhang [b], Sen Yang [a], Qingzhi Yan [a, *], Zhiyuan Hong [a], Min Xia [a], Changchun Ge [a]

[a] Institute of Nuclear Materials, University of Science and Technology Beijing, 30 Xueyuan Road, Haidian District, Beijing, 100083, China
[b] China Nuclear Power Technology Research Institute, Shenzhen, 518000, China

ARTICLE INFO

*Article history:*
Received 14 November 2016
Received in revised form
23 July 2017
Available online 3 August 2017

*Keywords:*
Ferritic/martensitic steels
Creep behavior
Microstructure evolution

ABSTRACT

Creep behaviors of CNS-2 steel have been investigated under different conditions at 600–650 °C and 105–180 MPa, and the microstructures and precipitations of crept and aged specimens have been characterized. It is showed that the CNS-2 steels have remarkable creep resistance at 600°C/105MPa until at least 1500 h, and the accelerated creep occurs at the elevated temperature of 650 °C and applied stress of 180MPa. The CNS-2 steels are toughened after creep without hardening and embrittlement. Their grain microstructures are stable but the sub-structures change during the creep. The subgrains coarsen with creep strain and the density of dislocations decreases due to the recovery at elevated temperature. Three kinds of precipitations including $M_{23}C_6$, MX-type carbonitride and Laves phase are identified in the crept steels by TEM, EDS and SEAD analysis. It is also found that the applied stress promotes the precipitations formed at the grain or subgrain boundary.



## 1. Introduction

High-Cr (9–12 wt%) ferritic/martensitic steels have been widely used as structural materials in nuclear reactors for their excellent high-temperature mechanical properties and corrosion resistance [1,2]. They are also selected as the most promising candidate materials for the in-core components of next generation advanced nuclear systems, because of their superior thermal conductivity, thermal expansion and radiation-induced swelling resistance compared to austenitic steels [3–6]. However, when the operating temperature in reactor is elevated over 600 °C, the high-temperature properties of conventional F/M steels suffer a significant degradation during the long-term creep, which is the primary limitation of the utilization of these steels [7,8]. Recently, several versions of advanced F/M steels have been developed with the aim to enhance the creep resistance [9,10]. For instance, the creep resistance of a 9 per-cent Cr martensitic steel is significantly improved using nano-sized carbonitride dispersions [11]. Addition and optimization of low active alloying elements lead to plenty of RAFM steels with remarkable creep strength such as 9Cr2WVTa [12], Eurofer-97 [13–15], F82H [16,17], JLF-1 and CLAM steels [18,19]. Thermo-mechanical-treatment processing are introduced into steel fabrication and their creep properties are further improved by controlling of microstructure [20]. Mechanically alloyed ODS steels also exhibit high resistance to creep deformation which are derived from the presence of thermal stable nano-sized oxide particles and nanoclusters at elevated temperature [21–26].

China Nuclear Steel-2 (CNS-2) is a kind of modified F/M steel developed by our group, for the utilization in nuclear applications at elevated temperature about 600–650 °C. The steel is designed as a 12%Cr-type steel for the requirement of corrosion-resistance, and their high-temperature mechanical property is expected to be improved by the alloying elements such as Mo, W, V and Ta. For instance, the simultaneous addition of Mo and W have a more beneficial effect on the high-temperature strength and creep resistance than adding them alone [27]. V and Ta are found to reduce the grain size due to the formation of dispersed and refined MX-type (M = Ta,V; X = C,N) precipitations [28]. In our previous results, the steel achieved high ultimate tensile strength of 925 MPa at room temperature and 483 MPa at 600 °C, and the elongation of~20% indicated the adequate ductility for the processing of thin-wall tube [29]. Additionally, the steel showed significantly low swelling of 0.057% and 0.25% under 5MeV $Fe^{2+}$ ion irradiation up to 450dpa at 460 °C with 10 appm and 100 appm pre-

* Corresponding author.
*E-mail address:* qzyan@ustb.edu.cn (Q. Yan).

http://dx.doi.org/10.1016/j.jnucmat.2017.08.003
0022-3115/

**Table 1**
Chemical composition of CNS-2 steel (wt.%).

| C | Cr | Mo | W | Mn | Ni | Si | V | Ta | N | Al | B | S/P | Fe |
|---|---|---|---|---|---|---|---|---|---|---|---|---|---|
| 0.1 | 12.0 | 1.0 | 1.1 | 1.0 | 1.0 | 0.17 | 0.2 | 0.15 | 0.06 | 0.02 | 0.001 | <0.005 | Bal. |

implanted helium, respectively [30,31]. It suggested a promising development for the irradiation-resistant materials such as fuel claddings and fusion blankets. However, the long-term properties at elevated temperature are still missing to exhaustively evaluate the new developed steel. In this paper, we focused on the creep behaviors of CNS-2 steels at different temperature and stress conditions, and their microstructures were also characterized for the further understanding of the steels during creep.

## 2. Experimental

### 2.1. Materials and heat treatment

The actual chemical composition in mass percent of CNS-2 steel is listed in Table 1. The ingot was casted by vacuum induction melting (VIM) method and then forged into a bar with cross section of 90 × 60mm. The bar was subsequently hot rolled into 15mm thick plates at the temperature range of 1100 to 900 °C followed by water spray cooling. The plates were quenched and tempered to obtain best match of strength and toughness. The details of heat treatment were as follows: austenitizing at 1000 °C for 30min followed by water quenching, then tempering at 780 °C for 120min followed by air cooling.

### 2.2. Creep test

According to Chinese Standard of GB/T 2039-1997, creep specimens with a gauge length of 100mm and a diameter of 10mm were cut from the as-heat-treatment plate by electron discharged machine. Three different creep conditions of (1) 600°C/105MPa, (2) 650°C/105MPa, (3)650°C/180MPa were selected to study the creep behavior of the steel under different temperatures and stresses. After creep test, specimens taken from grip portion and gauge portion were both prepared for the following tests, including impact test, hardness test and microstructure examination, for a comparison of thermal aging state and creep state.

### 2.3. Impact and hardness tests

As-received and crept (grip portion and gauge portion) specimens were prepared for impact test, with the size of 27 × 4 × 3mm and a V-notch in the middle of the specimens. The impact test was carried out at room temperature and the impact energy values were used for toughness evaluation. Brinell hardness of each specimen from grip portion and gauge portion under different creep conditions was measured under 187.5kgf load with 10s duration using XHB-3000 Brinell hardness testing machine.

### 2.4. Microstructure examination

The microstructures of specimens before and after creep test were observed by optical microscope (OM). All the specimens were polished using standard metallographic technique and etched with 5ml HF + 95ml $HNO_3$ solutions. Transmission electron microscopy (TEM), energy dispersive spectroscopy (EDS) and selected area electron diffraction (SAED) were used for the characterization of the subgrain structures and the precipitations. The TEM samples were prepared by conventional twin-jet electropolishing.

## 3. Results

### 3.1. Creep behavior

The creep behavior of CNS-2 steels is characterized by the relationship of strain, time and creep rate that strongly depends on testing temperature and stress conditions. The creep rupture results of CNS-2 steel specimens crept at various conditions are quite different. The specimen crept at 600°C/105MPa keeps low strain of <1% after 1500h, while the specimen crept at 650°C/105MPa is elongated to 7% after 800h, but they both didn't rupture at the end of creep test. However, the specimen crept at 650°C/180MPa quickly failed only after 8 h with the elongation of ~4%. The strain-time curves tested at 600°C/105MPa and 650°C/105MPa are shown in Fig. 1. The corresponding creep rate-time data are shown in Fig. 2, where the scatter problem is removed by average treatment of measured data (gray dots). For the specimen crept at 650°C/180MPa, there is no creep curve available due to its limited data. As seen in Figs. 1 and 2, the specimen crept at 600°C/105MPa shows an initial creep rate of ~0.01%·$h^{-1}$ at the primary stage and a gradually decrease to ~$10^{-4}$%·$h^{-1}$. Even though after 1500h, the strain is maintained less than 1% with no tendency of accelerated creep, showing remarkable creep resistance. As for the specimen crept at 650°C/105MPa, the creep rate decreases gradually from an initial rate of ~0.03%·$h^{-1}$ to the minimum creep rate of ~0.002%·$h^{-1}$ at about 300h, then it increases rapidly in the tertiary creep regime, with a strain of ~7% at the end of the curve. It should be noted that the creep data here are based on the engineering stress and strain records. However, under constant load condition, the true stress is increasing with true strain for constant specimen volume, as

$$\sigma_{true} = \left(\frac{F}{S_0}\right) e^{\varepsilon_{true}} \quad (1)$$

where $\frac{F}{S_0}$ is the initial stress. After conversion from engineering data to true one, the $\dot{\varepsilon}_{true} - \varepsilon_{true}$ curve is plotted in Fig. 3. As shown, only a minor difference between the engineering and the true data for small strains. The curves obtained for 105 MPa at 600 °C and 650 °C

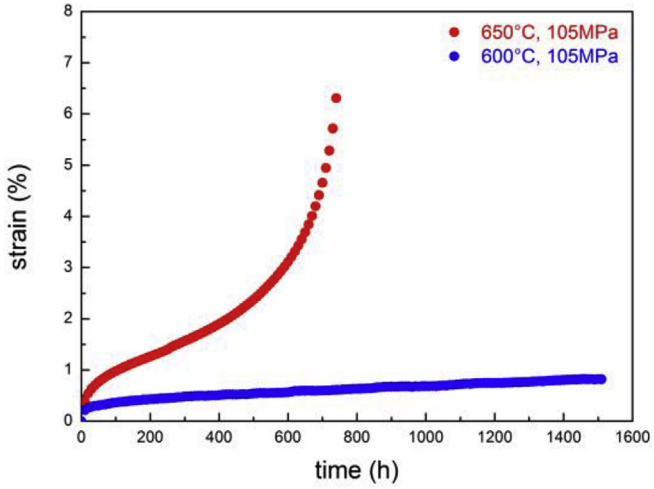


**Fig. 1.** Strain-time creep curves of CNS-2 steel at 600°C/105MPa and 650°C/105MPa.

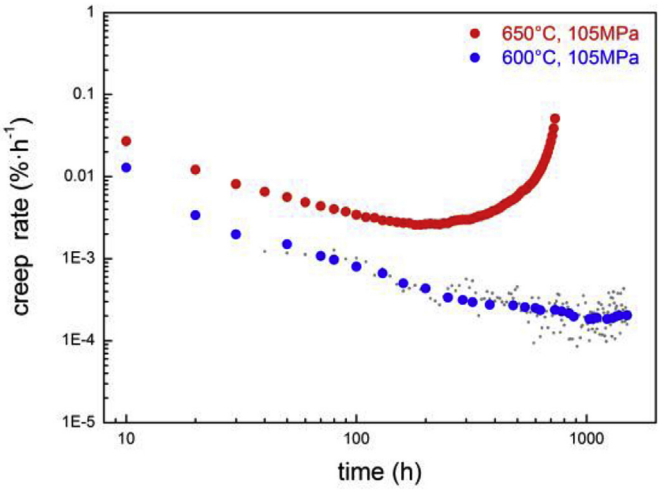


**Fig. 2.** Creep rate-time creep curves of CNS-2 steel at 600°C/105MPa and 650°C/105MPa.

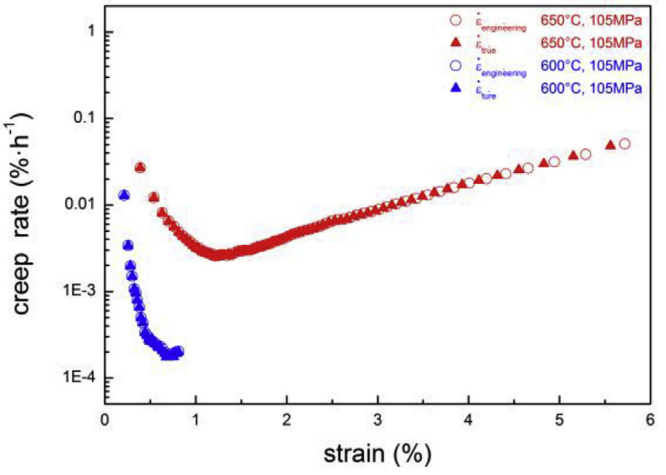


**Fig. 3.** Engineering/ture creep rate of CNS-2 steel as function of engineering/true strain at 600°C/105MPa and 650°C/105MPa.

run parallel with the strain less than ~1%. For the 650°C/105MPa curve, there is no steady state but transient hardening followed by transient softening with a minimum creep rate in between. At the lower temperature of 600 °C, the creep rate is one order lower than 650 °C at the same strain. However, the minimum creep rate is not obtained because of the much slower creep. More testing time is required to reach the same strain.

### 3.2. Hardness and toughness

The Brinell hardness data of as-received and creep-tested specimens (including grip portion and gauge portion) are listed in Table 2. It shows a distinct hardness reduction of the steel from 315 HBW to 245, 235, 200 HBW, corresponding to three creep conditions of 600°C/105MPa, 650°C/105MPa and 650°C/180MPa, respectively, which is attributed to the softening of the materials at elevated creep temperature. In addition, the hardness in grip portion (aging state) and gauge portion (creep state) display slight difference, which implies that the applied stress has little effects on the hardness of the crept specimens.

The impact energy of creep-tested specimens is summarized in Table 3. As can be seen, the impact energy of the specimens increase after creep tests, and is generally higher in gauge portion than in grip portion. The specimens crept at 650°C/105MPa presents the highest impact energy among the three creep conditions, no matter in gauge portion or in grip portion. This indicates that the steels were toughened during the creep and the toughness was affected by the creep temperature and applied stress. Actually, the changes of hardness and toughness are related to the evolution of the microstructure of the steels, which is examined in the following section.

### 3.3. Microstructure evolution and precipitation characterization

The optical images of as-received and creep-tested specimens are shown in Fig. 4. The microstructures of as-received specimen are common tempered martensitic structures with pockets and blocks (Fig. 4a). A few (~4%) elongated δ-ferrite exist due to the high contents of ferrite-formation alloying elements such as Cr, Mo and W, which cause the incomplete austenitizing during the heat-treatment. The size of prior-austenitic grains are in the range of 10–30μm. Even though after long-time creep at 600°C/105MPa/1500h and 650°C/105MPa/800h, the matrix remains similar grain size and morphology, as shown in Fig. 4b–c.

Unlike the stability of grain-scale microstructures, the subgrain-scale structures change under different creep conditions. The subgrain size distributions of as-received and crept specimens are given in Fig. 5. For as-received specimens, the average subgrain size is 0.53μm and increase to 0.79μm, 1.40μm and 1.27μm after creep testing at 600°C/105MPa, 650°C/105MPa and 650°C/180MPa, respectively. There are only two types of precipitation: coarse Cr-rich $M_{23}C_6$(100–200nm) and fine MX(20–50nm) located on the subgrain/lath boundaries or distributed in the subgrains, but Laves phases are not detected. After creep, precipitations of $M_{23}C_6$ and MX still exist in the matrix with slight growth. It is noticed that large Laves phases are found in the crept samples (Fig. 6b–d); their size and amount are related to their creep conditions. The size and amount of Laves phases in the specimens crept at 600°C/105MPa are obviously greater than that in other specimens, which is probably due to the longest creep time of 1500h.

EDS and SEAD analysis are performed on the crept specimens of 600°C/105MPa/1500h to confirm the details of the precipitations. The results demonstrate that large gray rod-like precipitations and deep dark block-like particles are Cr-rich $M_{23}C_6$ and $Fe_2W$ Laves phase respectively, which are mostly located near the grain/lath boundaries; and the distributed finer near-spherical particles are identified as TaC precipitations, as shown in Fig. 7.

**Table 2**
Brinell hardness of specimens at grip and gauge portions before and after creep tests.

| | As-received | Creep-tested | | | |
|---|---|---|---|---|---|
| | | | 600°C/105MPa | 650°C/105MPa | 650°C/180MPa |
| Brinell hardness/HBW | 315 | gauge portion(creep state) | 246 | 239 | 203 |
| | | grip portion(aging state) | 243 | 235 | 196 |

**Table 3**
Impact energy of specimens at grip and gauge portions before and after creep tests.

| | As-received | Creep-tested | | | |
|---|---|---|---|---|---|
| | | | 600°C/105MPa | 650°C/105MPa | 650°C/180MPa |
| Impact energy /J | 5.5 | gauge portion(creep state) | 8.5 | 11.0 | 10.0 |
| | | grip portion(aging state) | 6.0 | 8.0 | 7.5 |

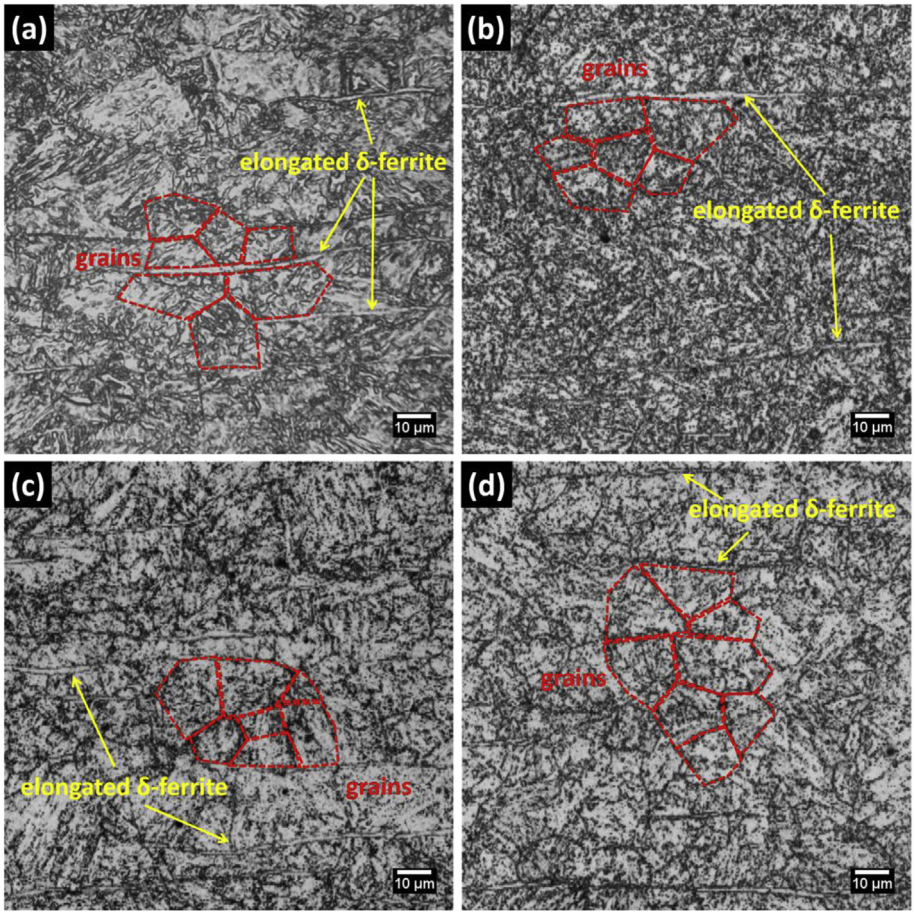


**Fig. 4.** The OM microstructure of as-received and crept specimen of CNS-2 steel.
(a)as-received, (b)600°C/105MPa, 1500h, (c)650°C/105MPa, 800h, (d)650°C/180MPa, 8h.

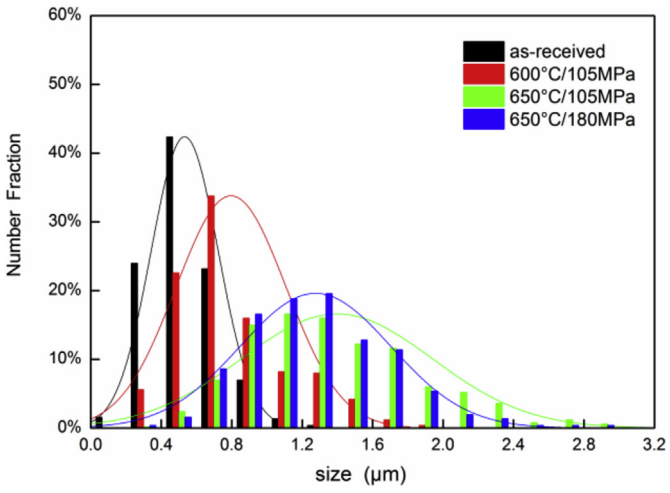


**Fig. 5.** Subgrain size distributions of as-received and crept specimens of CNS-2 steel.

To investigate the effect of creep stress on the microstructures of steel, two specimens in both gauge portion and grip portion were observed by TEM. As seen in Fig. 8, it appears that the precipitations, especially the Laves phase, prefer to locate on the grain or subgrain boundaries (Fig. 8a, c and 8e), corresponding to the three stressed conditions. But under the unstressed condition, precipitations are mostly dispersed in the grain (Fig. 8b, d and 8f). The size and amount of precipitations in gauge portion are larger than those in grip portion. This phenomenon can be explained by the change of dislocation density. Dislocations, which acting as the nucleation sites for precipitations, can be promoted by creep stress to move and pile up at the grain boundary, leading to the nucleation of precipitations at the grain boundary and then grow up.

## 4. Discussion

As shown in Fig. 3, $\dot{\varepsilon}_{true}$ increases with strain beyond a relative minimum at about 0.013. It is commonly assumed that the increase of $\dot{\varepsilon}_{true}$ in the tertiary stage of creep is due to fracture. To qualify the

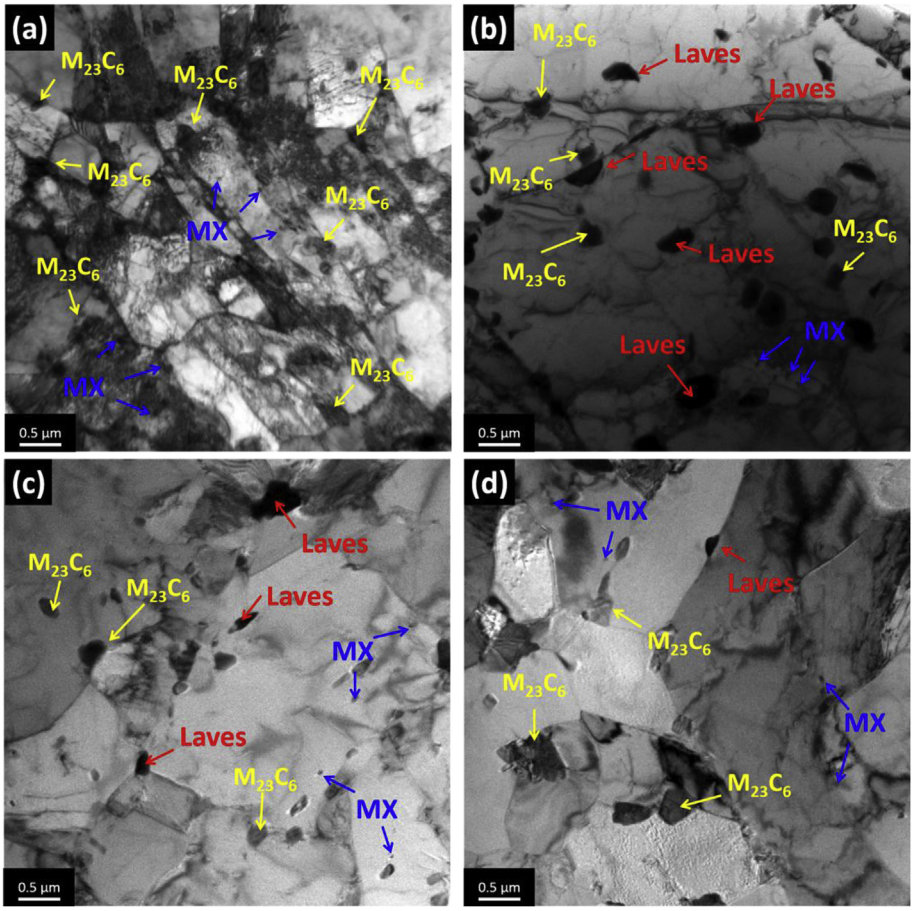


**Fig. 6.** The TEM microstructure of as-received and crept specimen of CNS-2 steel: (a)as-received, (b)600°C/105MPa, 1500h, (c)650°C/105MPa, 800h, (d)650°C/180MPa, 8h.

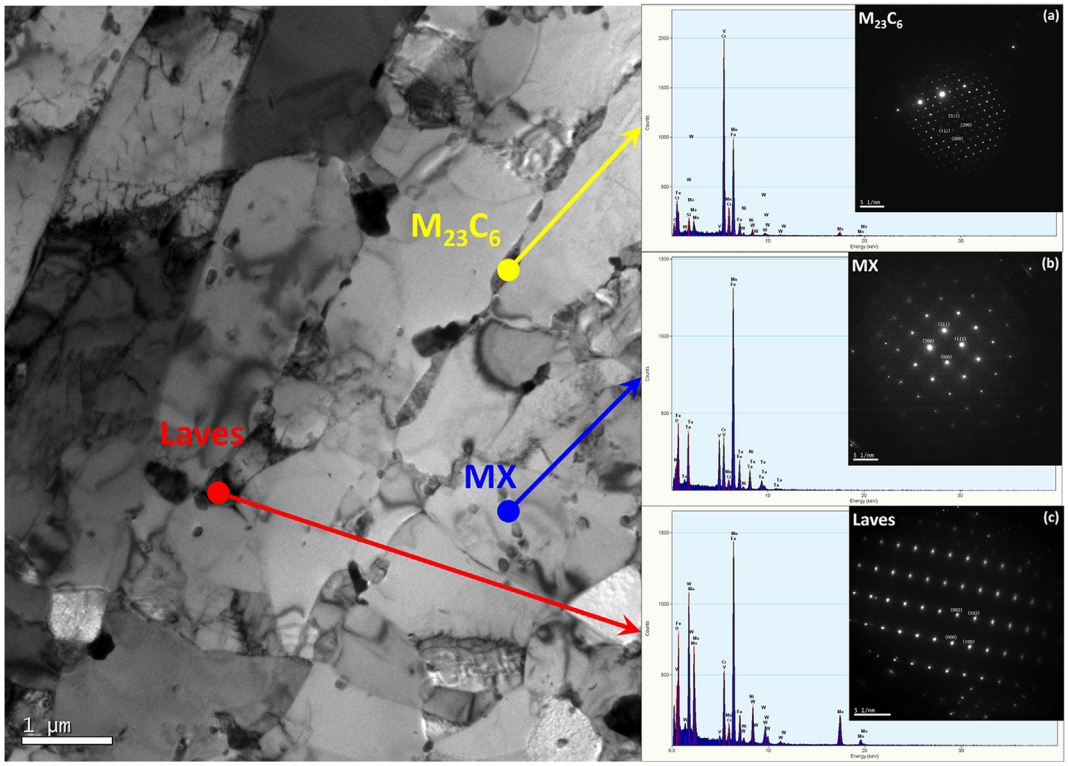


**Fig. 7.** EDS and SEAD characterization of precipitations in the creep-tested CNS-2 steel at 600°C/105MPa: (a)Cr-rich $M_{23}C_6$, (b)Ta-rich MX, (c)$Fe_2W$ Laves phase.

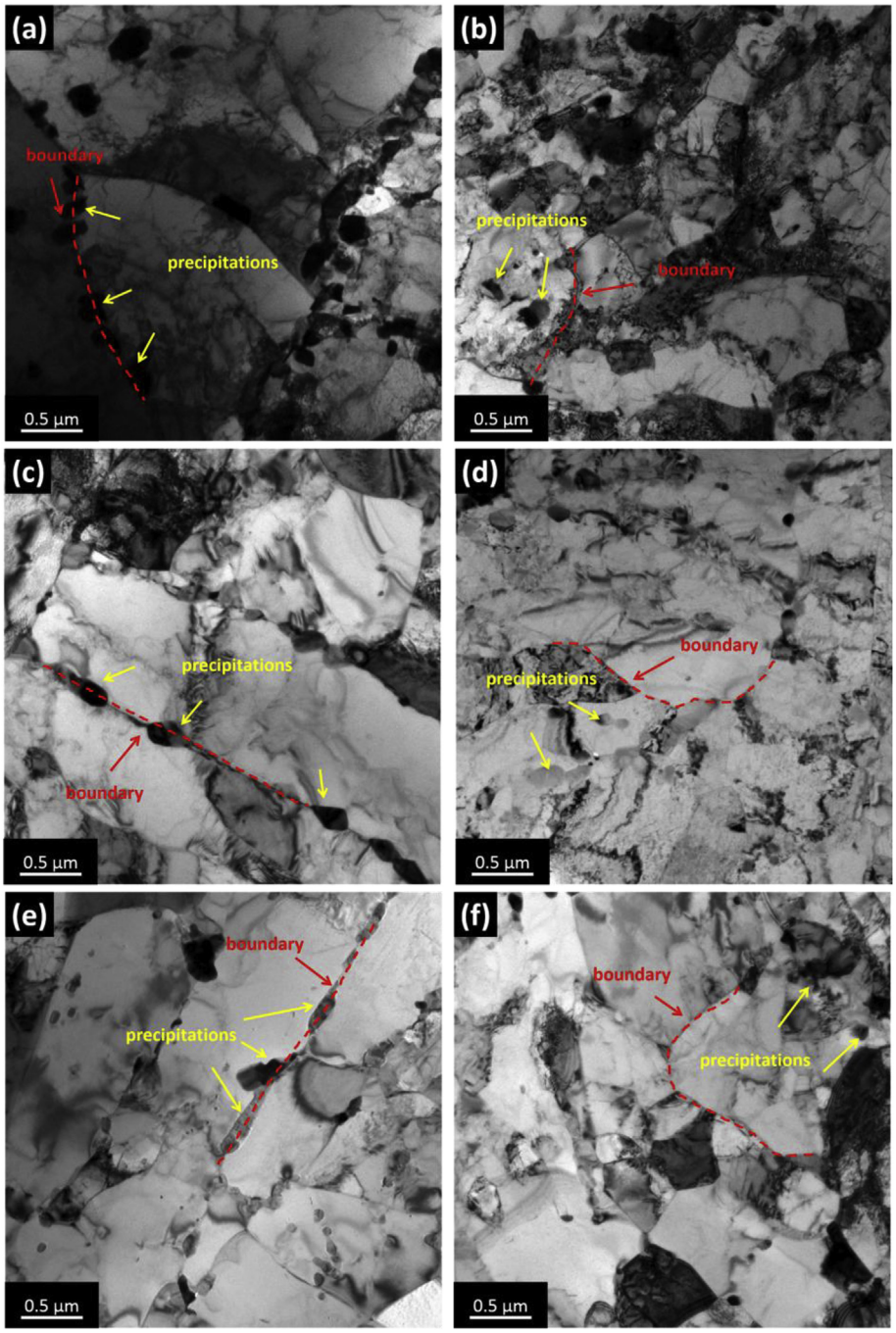


**Fig. 8.** TEM micrographs of specimens in creep and aging conditions:
(a) 600°C/105MPa/1500h, gauge.
(b) 600°C/105MPa/1500h, grip.
(c) 650°C/105MPa/800h, gauge.
(d) 650°C/105MPa/800h, grip.
(e) 650°C/180MPa/8h, gauge.
(f) 650°C/180MPa/8h, grip.

onset of significant fracture influence on $\dot{\varepsilon}_{true}$, the slope of $\log\dot{\varepsilon}_{true} - \varepsilon_{true}$ curve is determined as

$$\mathbf{n}' = \frac{\Delta \log \dot{\varepsilon}_{true}}{\Delta \varepsilon_{true}} \tag{2}$$

and $\mathbf{n}' - \varepsilon_{true}$ curve is plotted in Fig. 9. If that were the case, the slope n' would monotonically increase to infinity. This is not the case. Instead, n' reaches relative maximum of 36 and thereafter declines. Therefore the steep increase of $\dot{\varepsilon}_{true}$ with $\varepsilon_{true}$ must be explained in terms of increase of true stress $\sigma_{true}$ with strain (specimen becomes thinner in tensile creep) and microstructural softening. In the first case n' should equal the stress exponent n of the creep rate in the steady state at constant precipitate structure [32]. However, a value of n' = 36 at about 100 MPa seems to be distinctly larger than expected values of the stress exponent n of

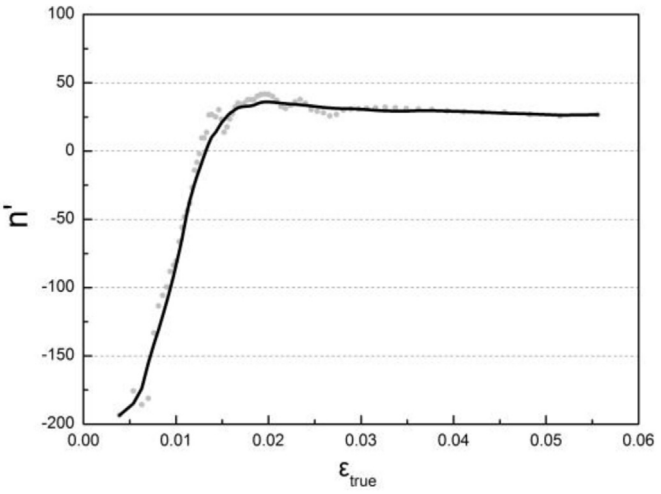


**Fig. 9.** Slope n' versus true strain $\varepsilon_{true}$ curve at 650°C/105MPa.

**Table 4**
Mean subgrain size of CNS-2 steel at different creep strain.

| | As-received | Creep-tested | | |
|---|---|---|---|---|
| | | 600°C/105MPa | 650°C/105MPa | 650°C/180MPa |
| Creep strain | 0 | <1% | 7% | 4% |
| Mean subgrain size | 0.53μm | 0.79μm | 1.40μm | 1.27μm |

the steady state creep rate. This indicates that microstructural softening is involved, too. As the density of free dislocations reaches a dynamic equilibrium of storage and recovery within a few percent of strain, the probably causes of softening are sub-grain growth and loss in particle strengthening.

As mentioned before, the CNS-2 steels have tempered martensitic structures with refined grains, dispersed precipitations and high density of dislocations that result from the pre-deformation and martensitic transformation. It is also understood that the steels are strengthened by the subgrains and particles, which lead to small initial creep strain and creep rate at the beginning of creep tests. As usual, the creep behavior of materials is related to their creep strength, which is strongly affected by the microstructure evolution during creep, such as subgrains coarsening, dislocations recovery or precipitate formation. For 9–12%Cr martensitic steels, it is reported that the subgrain structures are important strength-controlling elements and develop with the creep strain [7,33,34]. In order to find the relationship between subgrain growth and creep behavior of the CNS-2 steels, the correspondence of subgrain size and creep strain is listed in Table 4. It indicates that the coarsening of subgrain is not enough when the strain is very small. So the subgrain-strengthening is maintained in the transient creep region until reaching the minimum creep rate. After that, subgrains coarsen at the relative large strain, resulting in a decrease of creep strength. The drop of deformation resistance causes more increase of creep rate and strain, showing the acceleration creep region. It is obviously shown in Fig. 3 for the creep curves of 650°C/105MPa specimen. But at lower temperature of 600 °C, the subgrain coarsening is weaker than at the higher temperature, and it is not enough for the coarsening at the less strain.

Emphasizing the subgrains does not mean that particles are unimportant. Actually, the migration of subgrain boundaries are hindered by the particles and the subgrain coarsening is suppressed. The decreased hardness and increased toughness of the crept specimens is also related to the subgrain coarsening and precipitations evolution under various temperatures and stresses. New-formed Laves phase particles, as the obstacles to pin the dislocations and grain boundaries, enhance the precipitation strengthening effect and improve the deformation resistance. However, this strengthening effect is related to the amount, size and distribution of second phase particles. According to the thermodynamic equilibrium calculations of the CNS-2 steels in Fig. 10, the mole percent of Laves phases is decreased from 600 °C to 650 °C, which is in accordance with the TEM observation in Fig. 6b–d. The Laves phase particles in specimens crept at 600 °C are larger than that at 650 °C, which cause the lower toughness. And at the same temperature of 650 °C, the toughness of specimens under 180MPa are lower than that under 105MPa, because the

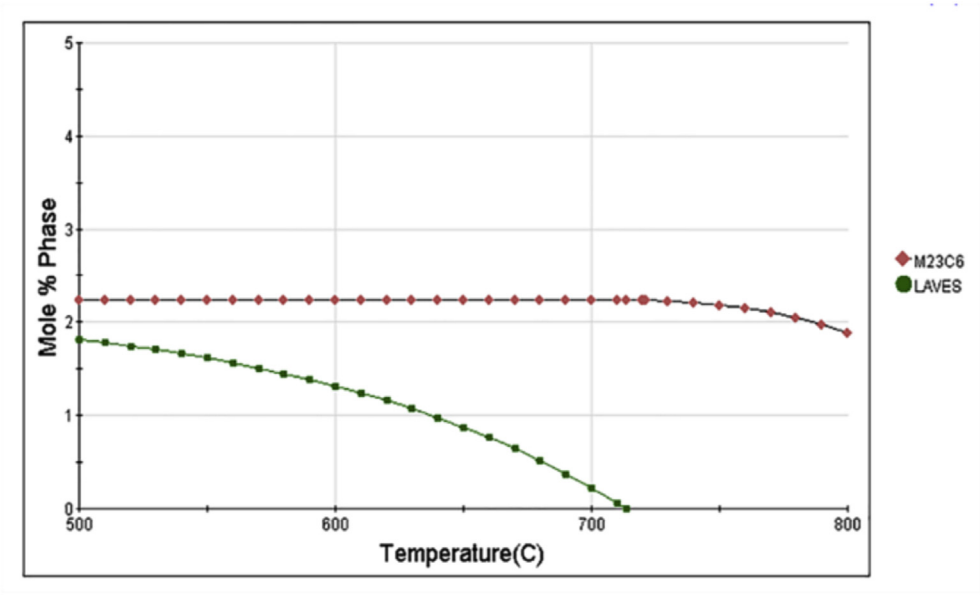


**Fig. 10.** Thermodynamic equilibrium calculations of phase fraction of CNS-2 steels.

precipitations tend to form at grain boundaries under higher stress level and the strengthening effects are reduced. Compared to the stressed specimens, the lower toughness of unstressed specimens may be attribute to the unsettled temperature in grip portion.

## 5. Conclusions

Creep behaviors of CNS-2 steel are investigated at three creep condition: (1) 650°C/180MPa, (2) 650°C/105MPa, (3) 600°C/105MPa. Hardness and impact tests, microstructure observation and precipitations characterization are performed on the as-received, crept (grip portion and gauge portion) specimens. The results are as follows:

(1) The CNS-2 steel shows remarkable creep resistance at 600°C/105MPa, keeping the low creep strain less than 1% without any trend of creep acceleration after crept over 1500h. When the temperature is elevated to 650 °C, the creep resistance is weak and the creep curve exhibits V-like shape. At higher stress level of 650 °C/180MPa, the material failure occurs only after 8 h. The CNS-2 steels are softened and toughened without hardening and embrittlement after creep tests at 600–650 °C and 105–180MPa.
(2) The creep behaviors and mechanical properties of CNS-2 steel are related to the microstructure evolution during the creep. The grain-scale microstructure of CNS-2 steel is stable but substructure changes during the creep. The materiels are softened due to subgrain coarsening with increase of strain at elevated temperature, which is partly compensated by the precipitation hardening.
(3) Cr-rich $M_{23}C_6$ and Ta-rich MX precipitations are identified in the as-received and creep-tested specimens. Laves phase is not found in the as-received specimen but precipitates during the creep as a strengthening phase to the CNS-2 steel.
(4) The applied stress promotes the formation of the precipitations at the grain or subgrain boundaries, especially for formation of Laves phases after long-term creep. The inhomogeneous distribution of precipitations aggravates the creep deformation of CNS-2 steel under high stress level.

## Acknowledgements

The authors gratefully acknowledge the financial support of ITER National Magnetic Confinement Fusion Program (No.2014GB123000) and the National Key Research and Development Program of China (No.2017YFB0702400).

## References

[1] S.J. Zinkle, J.T. Busby, Structural materials for fission and fusion energy, Mater. Today 12 (2009) 12–19.
[2] G.S. Was, P. Ampornrat, G. Gupta, S. Teysseyre, E.A. West, T.R. Allen, K. Sridharan, L. Tan, Y. Chen, X. Ren, Corrosion and stress corrosion cracking in supercritical water, J. Nucl. Mater. 371 (2007) 176–201.
[3] R.L. Klueh, A.T. Nelson, Ferritic/martensitic steels for next-generation reactors, J. Nucl. Mater. 371 (2007) 37–52.
[4] T.R. Allen, J.T. Busby, R.L. Klueh, S.A. Maloy, M.B. Toloczko, Cladding and duct materials for advanced nuclear recycle reactors, Jom - J. Minerals Metals Mater. Soc. 60 (2008) 15–23.
[5] S.J. Zinkle, G.S. Was, Materials challenges in nuclear energy, Acta Mater. 61 (2013) 735–758.
[6] K.L. Murty, I. Charit, Withdrawn: structural materials for Gen-IV nuclear reactors: challenges and opportunities, J. Nucl. Mater. 383 (2008) 189–195.
[7] F. Abe, S. Nakazawa, H. Araki, T. Noda, The role of microstructural instability on creep behavior of a martensitic 9Cr-2W steel, Metallurgical Mater. Trans. A 23 (1992) 469–477.
[8] S.J. Zinkle, N.M. Ghoniem, Operating temperature windows for fusion reactor structural materials, Fusion Eng. Des. 51 (2000) 55–71.
[9] R.L. Klueh, D.S. Gelles, S. Jitsukawa, A. Kimura, G.R. Odette, B.V.D. Schaaf, M. Victoria, Ferritic/martensitic steels – overview of recent results, J. Nucl. Mater. 307–311 (2002) 455–465.
[10] R.L. Klueh, Elevated temperature ferritic and martensitic steels and their application to future nuclear reactors, Int. Mater. Rev. 50 (2013) 287–310.
[11] M. Taneike, F. Abe, K. Sawada, Creep-strengthening of steel at high temperatures using nano-sized carbonitride dispersions, Nature 424 (2003) 294–296.
[12] R.L. Klueh, Reduced-activation steels: future development for improved creep strength, J. Nucl. Mater. 378 (2008) 159–166.
[13] R. Lindau, A. Möslang, M. Schirra, Thermal and mechanical behaviour of the reduced-activation-ferritic-martensitic steel EUROFER, Fusion Eng. Des. 61 (2002) 659–664.
[14] A.M. Lancha, J. Lapeña, R. Lindau, Creep strength of reduced activation ferritic/martensitic steel Eurofer'97, Fusion Eng. Des. 75 (2005) 1003–1008.
[15] G. Yu, N. Nita, N. Baluc, Thermal creep behaviour of the EUROFER 97 RAFM steel and two European ODS EUROFER 97 steels, Fusion Eng. Des. 75–79 (2005) 1037–1041.
[16] S. Jitsukawa, M. Tamura, B.V.D. Schaaf, R.L. Klueh, A. Alamo, C. Petersen, M. Schirra, P. Spaetig, G.R. Odette, A.A. Tavassoli, Development of an extensive database of mechanical and physical properties for reduced-activation martensitic steel F82H, J. Nucl. Mater. s 307–311 (2002) 179–186.
[17] K. Shinozuka, H. Esaka, H. Sakasegawa, H. Tanigawa, Creep strength and microstructure of F82H steels near tempering temperature, J. Nucl. Mater. 464 (2015) 155–159.
[18] Y. Li, T. Nagasaka, T. Muroga, Creep properties and microstructure of JLF-1 and clam steels aged at 823 to 973 K, Fusion Sci. Technol. 56 (2009) 323–327.
[19] Y.F. Li, T. Nagasaka, T. Muroga, Q.Y. Huang, Y.C. Wu, Effect of thermal ageing on tensile and creep properties of JLF-1 and CLAM steels, J. Nucl. Mater. 386 (2009) 495–498.
[20] L. Tan, D.T. Hoelzer, J.T. Busby, M.A. Sokolov, R.L. Klueh, Microstructure control for high strength 9Cr ferritic–martensitic steels, J. Nucl. Mater. 422 (2012) 45–50.
[21] R. Lindau, A. Möslang, M. Schirra, P. Schlossmacher, M. Klimenkov, Mechanical and microstructural properties of a hipped RAFM ODS-steel, J. Nucl. Mater s 307–311 (2002) 769–772.
[22] R.L. Klueh, P.J. Maziasz, I.S. Kim, L. Heatherly, D.T. Hoelzer, N. Hashimoto, E.A. Kenik, K. Miyahara, Tensile and creep properties of an oxide dispersion-strengthened ferritic steel, J. Nucl. Mater. s 307–311 (2002) 773–777.
[23] S. Ukai, T. Okuda, M. Fujiwara, T. Kobayashi, S. Mizuta, H. Nakashima, Characterization of high temperature creep properties in recrystallized 12Cr-ODS ferritic steel claddings, J. Nucl. Sci. Technol. 39 (2002) 872–879.
[24] H. Sakasegawa, S. Ohtsuka, S. Ukai, H. Tanigawa, M. Fujiwara, H. Ogiwara, A. Kohyama, Microstructural evolution during creep of 9Cr-ODS steels, Fusion Eng. Des. 81 (2006) 1013–1018.
[25] S. Ohtsuka, S. Ukai, H. Sakasegawa, M. Fujiwara, T. Kaito, T. Narita, Nano-mesoscopic structural characterization of 9Cr-ODS martensitic steel for improving creep strength, J. Nucl. Mater. s 367–370 (2007) 160–165.
[26] T. Muroga, T. Nagasaka, Y. Li, H. Abe, S. Ukai, A. Kimura, T. Okuda, Fabrication and characterization of reference 9Cr and 12Cr-ODS low activation ferritic/martensitic steels, Fusion Eng. Des. 89 (2014) 1717–1722.
[27] Y. Kadoya, B.F. Dyson, M. Mclean, Microstructural stability during creep of Mo- or W-bearing 12Cr steels, Metall. Mater. Trans. A 33 (2002) 2549–2557.
[28] L. Tan, T.S. Byun, Y. Katoh, L.L. Snead, Stability of MX-type strengthening nanoprecipitates in ferritic steels under thermal aging, stress and ion irradiation, Acta Mater. 71 (2014) 11–19.
[29] Y. Yang, Q.Z. Yan, M.A. Rong, G.E. Chang-Chun, Effect of heat treatment process on mechanical properties and microstructure of modified CNS-II F/M steel, J. Iron Steel Res. Int. 18 (2011) 65–70.
[30] X. Wang, A.M. Monterrosa, F. Zhang, H. Huang, Q. Yan, Z. Jiao, G.S. Was, L. Wang, Void swelling in high dose ion-irradiated reduced activation ferritic–martensitic steels, J. Nucl. Mater. 462 (2015) 119–125.
[31] X. Wang, Q. Yan, G.S. Was, L. Wang, Void swelling in ferritic-martensitic steels under high dose ion irradiation: exploring possible contributions to swelling resistance, Scr. Mater. 112 (2016) 9–14.
[32] W. Blum, J. Dvořák, P. Král, P. Eisenlohr, V. Sklenička, Effects of grain refinement by ECAP on the deformation resistance of Al interpreted in terms of boundary-mediated processes, J. Mater. Sci. Technol. 32 (2016) 1309–1320.
[33] J. Hald, Microstructure and long-term creep properties of 9–12% Cr steels, Int. J. Press. Vessels Pip. 85 (2008) 30–37.
[34] A. Aghajani, C. Somsen, G. Eggeler, On the effect of long-term creep on the microstructure of a 12% chromium tempered martensite ferritic steel, Acta Mater. 57 (2009) 5093–5106.